Simultaneous Measurement of Plasma Pressure Anisotropy with a Double-Pass Thomson Scattering Diagnostic System on the TST-2

Junichi HIRATSUKA[a)], Akira EJIRI, Makoto HASEGAWA[1)], Yoshihiko NAGASHIMA[1)], Keishun NAKAMURA, Yuichi TAKASE, Hiro TOGASHI, Hiroshi TOJO[2)], Takashi YAMAGUCHI and TST-2 group

The University of Tokyo, Kashiwa 277-8561, Japan
[1)]*Kyushu University, 6-1 Kasuga-koen, Kasuga, Fukuoka 816-8580, Japan*
[2)]*Japan Atomic Energy Agency, 801-1 Mukoyama, Naka-shi, Ibaraki 311-0193, Japan*

(Received 28 March 2014 / Accepted 3 October 2014)

We have developed a double-pass Thomson scattering diagnostic system for the TST-2 spherical tokamak device. By measuring the first- and second-pass scattering signals simultaneously, we obtained the two directional pressures and we measured the pressure anisotropy (i.e., the ratio of the pressures) with an error of 5% - 10% for moderate density ($\simeq 2 \times 10^{19}\,\mathrm{m}^{-3}$) plasmas. We observed 30% and 100% anisotropy at the center and edge of the Ohmic-heated plasmas, respectively. We propose a three-temperature Maxwellian model, in which the fitting is better than in the shifted-Maxwellian model. The estimated plasma current density was close to the averaged current density. The results suggest that the contribution of thermal electrons to a plasma current is large in Ohmic-heated plasmas.

Keywords: Thomson scattering, double-pass configuration, pressure anisotropy, current density measurement, TST-2

DOI: 10.1585/pfr.10.1402007

1. Introduction

The velocity distribution functions of plasma tend to be isotropic Maxwellian distribution functions when in equilibrium. In high temperature fusion plasmas, however, the distribution functions can be distorted due to various reasons, such as the electric field, the magnetic mirror effect, wave heating, and neutral beam injection. This anisotropy in the velocity distribution function results in a destabilization of the ballooning modes [1] and a deformation of the plasma pressure from the flux function [2]. Although anisotropy measurement is important, the diagnostics for the plasma core have not been established.

The Thomson scattering diagnostic is a method for measuring electron temperature and density from Thomson scattering light of a laser beam injected into a plasma. The wavelength spectrum of the scattering light reflects the Doppler shift of the electrons along the scattering vector $\boldsymbol{k} = \boldsymbol{k}_\mathrm{s} - \boldsymbol{k}_\mathrm{i}$ [3]. Here, $\boldsymbol{k}_\mathrm{s}$ and $\boldsymbol{k}_\mathrm{i}$ are the wave vectors of the scattered light and the injected laser, respectively. The width of the spectrum represents the electron temperature, and the intensity of the scattering light is proportional to the electron density. A method to measure the plasma pressure anisotropy with Thomson scattering diagnostics, proposed in 1979 [4], was discussed recently in detail [5,6]. Several experiments using Thomson scattering diagnostics have been performed to measure plasma pressure anisotropy and the shape of the plasma velocity distribution function [7–12]. These studies used visible high power lasers, that are not suitable for fusion plasma diagnostics. In addition, the reproducibility of the plasma discharge is still uncertain since $p_{\mathrm{e},\perp}$ and $p_{\mathrm{e},\parallel}$ were not measured simultaneously.

A two-directional plasma pressure diagnostic, the double-pass Thomson scattering diagnostic, with a Nd:YAG laser, was recently developed [13, 14]. The Nd:YAG laser is more appropriate than visible lasers due to its high repetition rate and its wavelength region (infrared). Furthermore, $p_{\mathrm{e},\perp}$ and $p_{\mathrm{e},\parallel}$ are measured almost simultaneously. In order to measure two-directional velocity distribution functions, the direction of $\boldsymbol{k}_\mathrm{s}$ or $\boldsymbol{k}_\mathrm{i}$ should be changed for each measurement. A laser beam passes through a plasma once in a standard Thomson scattering diagnostic. In contrast, the laser beam is reflected back to the plasma in the double-pass scheme. Then, the forward and the backward scattering light can be measured by single collection optics. Therefore, Thomson scattering lights with two directions of $\boldsymbol{k}_\mathrm{i}$ can be measured, and we can obtain the two-directional velocity distribution functions of the thermal electrons (Fig. 1).

However, there are problems for double-pass measurements using a Nd:YAG laser. First, the number of wavelength channels is restricted in Nd:YAG Thomson scattering because of the low signal level. Second, detec-

author's e-mail: hiratsuka.junichi@jaea.go.jp
[a)] Present address: Japan Atomic Energy Agency, 801-1 Mukoyama, Naka-shi, Ibaraki 311-0193, Japan

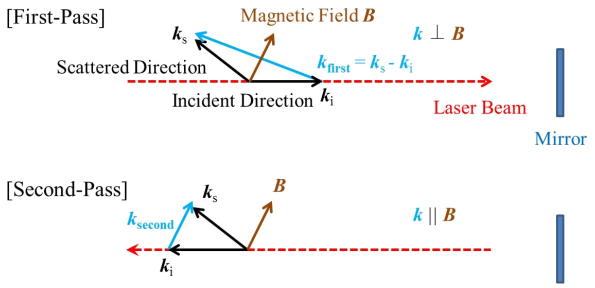

Fig. 1 Schematic of the geometry of double-pass Thomson scattering.

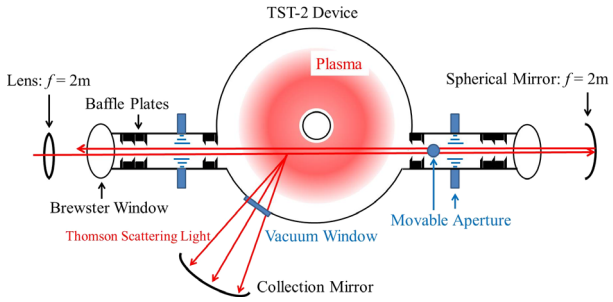

Fig. 2 Schematic of the laser path.

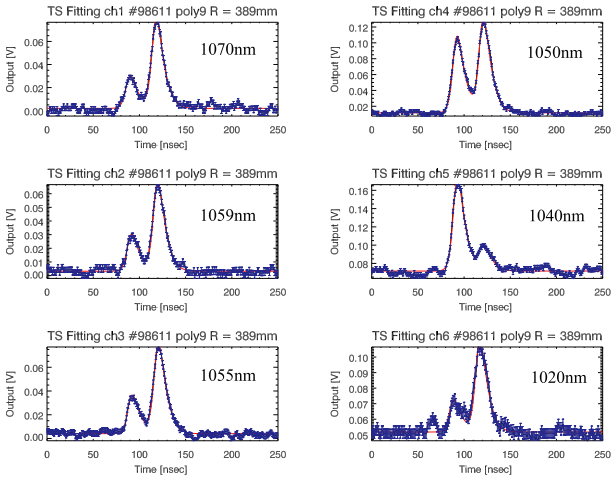

Fig. 3 Typical signals of a forward and a backward Thomson scattering light for each wavelength channel of a polychromator. Blue symbols with error bars represent signals with random noise including shot noise from stray light and thermal noise. Red curves denote fitting results to a template waveform [13].

tor and electric circuit must be fast-response and low-noise to separate the two pulses of the Thomson scattering lights within a very short time interval. In addition, we must consider the shape of the velocity distribution function when we apply this method to current density diagnostics. Although a current density profile was obtained in [12], the authors also reported that the estimation from the shifted-Maxwellian fitting was different from that of the moment of the velocity distribution in an Ohmic-heated plasma.

In this paper, we report an accurate diagnostic of pressure anisotropy with few wavelength channels by using a fast and low-noise detection system and by evaluating measurement error in detail. We also investigated the velocity distribution function in an Ohmic-heated plasma, and describe its application to current density measurement.

2. Double-Pass Thomson System

We have developed and previously reported a double-pass Thomson scattering diagnostic system [13, 14] on a TST-2 spherical tokamak device ($I_p \simeq 100$ kA, $B_t < 0.2$ T, $R_0 = 0.38$ m and $a = 0.25$ m) [15]. This system consists of laser injection optics, collection optics, and a detection system. We used a Nd:YAG laser with a beam energy of 1.6 J and a pulse width of 10 ns. The laser is injected into the plasma and reflected back by a spherical mirror (Fig. 2). The Thomson scattering lights, excited by the laser beam in the first- and second-passes, are collected by a spherical collection mirror (diameter 600 mm, focal length 300 mm) and then transferred into polychromators by fibers with a numerical aperture of 0.37. There are six wavelength channels in each polychromator. Each channel consists of an interference filter, an avalanche photodiode (Si APD S8890-30, Hamamatsu Photonics), and a two-stage amplifier. The detected signal is digitized by an oscilloscope. The forward- and backward-scattering pulses are separated clearly by a fast and low-noise detection system [16]. In this system, the velocity distribution functions that are nearly perpendicular and parallel to the magnetic field can be measured within 40 ns (Fig. 3). The forward and backward Thomson scattering signal intensities are estimated separately by fitting a superposition of two single-pass Thomson scattering waveforms. Details of the waveform fitting are described in [13].

Spectra obtained by the first- and second-passes reflect velocity distribution functions with different directions parallel to $\boldsymbol{k}_{\rm first}$ and $\boldsymbol{k}_{\rm second}$, respectively. $\boldsymbol{k}_{\rm first}$ and $\boldsymbol{k}_{\rm second}$ are the scattering vectors of the first- and second-passes, respectively. Furthermore, the scattering angles are different for the first- and second-passes. Spectra from a plasma with a temperature of 100 eV are plotted in Fig. 4, as are the sensitivities of each polychromator wavelength channel.

In order to prevent the laser beam from returning to the laser device, the returning laser path (second-pass) is displaced from the injecting laser path (first-pass). The measurement points in the first- (lower field side) and second-passes (higher field side) are about 10 mm apart, along the radial direction.

3. Error Estimation

Velocity distribution functions should be measured precisely for the diagnostics of pressure anisotropy and

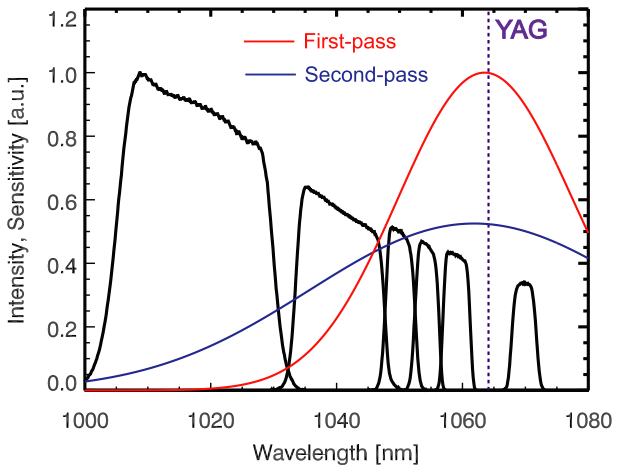

Fig. 4 Thomson scattering spectra measured by the first- (red) and second-passes (blue) from a plasma with an electron temperature of 100 eV. The sensitivities of the polychromator wavelength channels (see Fig. 3) are also plotted.

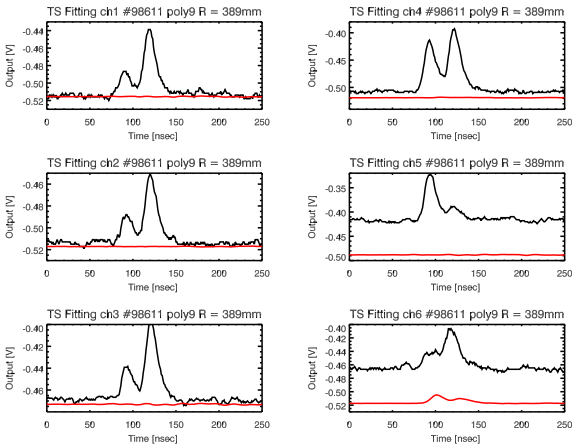

Fig. 5 Comparison of the intensity of the measured scattering signals (black) and the averaged stray light signals (red). The difference in DC levels between the black and the red curves represents the background plasma light.

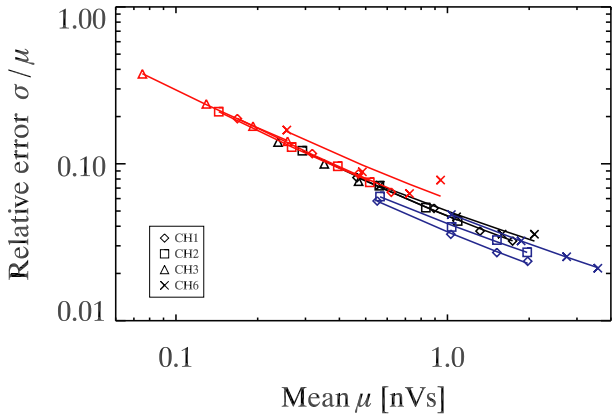

Fig. 6 Average vs. relative error of 1024 Raman scattering signals (double logarithmic plot).

plasma current density. However, the Thomson scattering signal is weak. Therefore, error estimation is important.

An error may be classified into systematic error and random error. The main sources of systematic error are variations in environmental temperature and bias voltage. These variations can pose problems because the sensitivity of the detector (APD) depends on these factors. With this system, the environmental temperature and bias voltage are controlled to an accuracy of less than 1°C and 0.5 V, respectively, which reduces the systematic error to 1.3%. Another systematic error comes from the 10 mm difference in the observation points for the forward and backward Thomson scattering measurements. The total systematic errors including these effects are 1.4% and 9.1% at $R = 389$ mm and $R = 220$ mm, respectively. On the other hand, the main sources of random noise are shot noise from stray signals, shot noise from a Thomson scattering signal, thermal noise [16], and errors in the waveform fitting. We reduced stray light with appropriate apertures (baffle plates and movable apertures in Fig. 2) to mask the stray light on the laser path. Figure 5 shows typical time-averaged stray light signals. We obtained the Thomson scattering signal by subtracting the averaged stray light signal from the measured signal. When we added all the wavelength channel signals, we found that the level of the stray light signal was less than about 5% of the Thomson scattering signal. The number of detected photons in the experiments described in this paper was at least more than 1000, which means that the error from the shot noise from stray light was less than 0.8%.

The dominant random noise sources were shot noise from Thomson scattering light, thermal noise, and error in the waveform fitting. The level of shot noise depends on the detected photon number, whereas thermal noise is independent of it. Therefore, total random noise σ_{random} can be expressed as

$$\sigma_{\mathrm{random}} = \sqrt{\eta_{\mathrm{shot}}\mu + \alpha_{\mathrm{thermal}}}, \quad (1)$$

where μ is the signal intensity. η_{shot} is a coefficient reflecting the shot noise, and α is a constant reflecting the thermal noise and the error in the waveform fitting. We estimated the constants by measuring the rotational Raman scattering of nitrogen. The scattering from nitrogen at constant pressure can be used as a light source of constant intensity. The average and standard deviation of 1024 Raman scattering signals correspond to μ and σ_{random}, respectively. Figure 6 shows the relation between the measured signal intensity and the random error values. We fitted the relation to the Eq. (1). Diamonds (⋄), squares (□), triangles (△), and crosses (×) represent the four wavelength channels of the polychromators. The black, red, and blue symbols indicate three different polychromators. The differences in the lines are caused by the difference in the sensitivities of

the polychromator channels.

The random error of each channel can be calculated from Eq. (1). For $n_e = 2 \times 10^{19}\,\mathrm{m}^{-3}$ (Fig. 3), the random errors in the electron temperature measured by the first- and second-passes ($T_{e,first}$ and $T_{e,second}$) are 2.4% and 4.5%, respectively, leading to a random temperature anisotropy error of $\Delta(T_{e,\perp}/T_{e,\parallel}) = 5.1\%$. As the systematic errors are about 1.4% and 9.1%, in this case, the total measurement errors were 5% and 10% at $R = 389$ mm and $R = 220$ mm, respectively.

4. Simulations and Models

The velocity distribution in an Ohmic-heated plasma is distorted by an external electric field along the toroidal direction [17]. Thus, a modeling of the distribution which expresses this distortion is necessary to reconstruct the distribution from the Thomson scattering signals. We calculated the velocity distribution function with the Fokker-Planck code CQL3D [18] for an Ohmic-heated plasma in the TST-2 device. In general, the shifted-Maxwellian is assumed for such a measurement. However, the calculation results suggest that there is no shift but the distribution is similar to that of Maxwellian's for different temperatures along $v_{e,\parallel} > 0$, $v_{e,\parallel} < 0$, and $v_{e,\perp}$. In order to represent such a distorted distribution, we propose a three-temperature Maxwellian model, in which the velocity distribution function is expressed as follows:

$$
\begin{aligned}
f_e(v_{e,\perp}) &= n_{e,\perp}\sqrt{\frac{m}{2\pi k T_{e,\perp}}}\exp\left(-\frac{m}{2kT_{e,\perp}}v_{e,\perp}^2\right),\\
f_e(v_{e,\parallel}>0) &= n_{e,co}\sqrt{\frac{m}{2\pi k T_{e,co}}}\exp\left(-\frac{m}{2kT_{e,co}}v_{e,\parallel}^2\right),\\
f_e(v_{e,\parallel}<0) &= n_{e,ctr}\sqrt{\frac{m}{2\pi k T_{e,ctr}}}\exp\left(-\frac{m}{2kT_{e,ctr}}v_{e,\parallel}^2\right).
\end{aligned}
\tag{2}
$$

Here, we defined the polarity as positive $v_{e,\parallel} > 0$ when the electron is co-directed with the acceleration direction of the Ohmic electric field. We refer to the $v_{e,\parallel} > 0$ and $v_{e,\parallel} < 0$ directions as the co- and counter- (ctr-) directions, respectively. Pressures are defined as $p_{e,\perp} = n_{e,\perp}T_{e,\perp}$, $p_{e,co} = n_{e,co}T_{e,co}$ and $p_{e,ctr} = n_{e,ctr}T_{e,ctr}$. Figure 7 shows a typical fitting result for a double-pass measurement into the three-temperature Maxwellian model. We obtained the data in a normal electric field discharge (blue in Fig. 9). $n_{e,first} = (2.07 \pm 0.03) \times 10^{19}\,\mathrm{m}^{-3}$ and $n_{e,second} = (2.06 \pm 0.06) \times 10^{19}\,\mathrm{m}^{-3}$, $T_{e,first} = 120 \pm 3\,\mathrm{eV}$ and $T_{e,second} = 135 \pm 6\,\mathrm{eV}$.

5. Experimental Results

We measured the pressure anisotropy of the Ohmic-heated plasma at the plasma center ($R = 389$ mm) and edge ($R = 220$ mm) on TST-2 with the double-pass Thomson scattering system. The scattering angles and the angle between the scattering vector $\boldsymbol{k}$ and the toroidal direction at each measurement point are listed in Table 1.

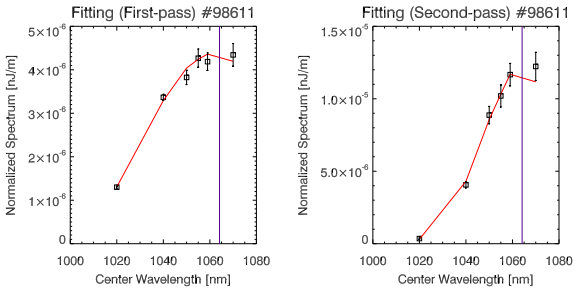

Fig. 7 A typical fitting result to the three-temperature Maxwellian model for the first- (left) and second- (right) pass scattering signals. Black squares with error bars denote the detected signals and red curves indicate the fitting results.

Table 1 The scattering angle (θ) and the angle between the scattering vector $\boldsymbol{k}$ and the toroidal direction (ϕ) at each measurement point.

R [mm]	θ_{first}	θ_{second}	ϕ_{first}	ϕ_{second}
220	138.9°	40.1°	128.2°	38.2°
389	124.7°	55.1°	91.3°	1.25°

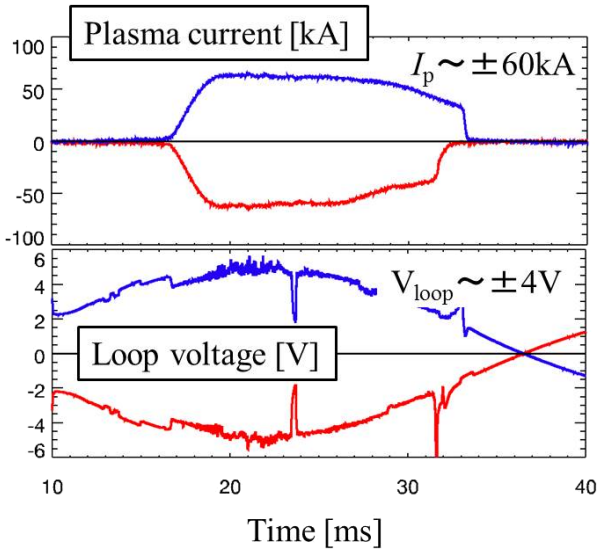

Fig. 8 Time slices of the total plasma current (I_p) and loop voltage (V_{loop}) of a typical Ohmic-heated plasma in TST-2 with normal (blue) and reversed (red) electric fields.

Since most of the signals reflect only one side of a velocity distribution function, as shown in Fig. 4, we can not measure $p_{e,co}$ and $p_{e,ctr}$ simultaneously. Therefore, we reversed the Ohmic electric field to invert the velocity distribution function of the plasma. Then, the plasma current is also reversed (Fig. 8). We then measured $p_{e,first}$ and $p_{e,second}$ at the plasma center and edge with normal and re-

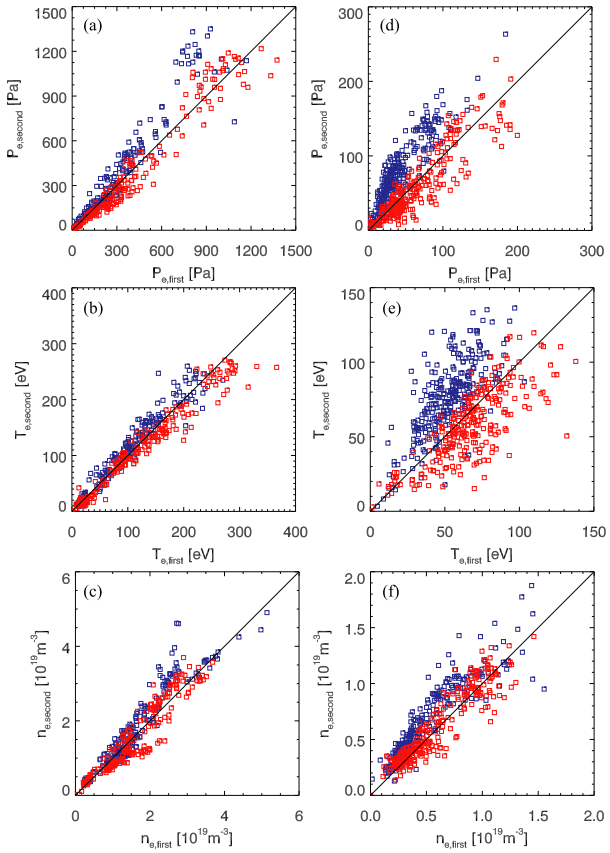

Fig. 9 Relationship between the parameters measured by the first- and the second-pass at the plasma center (R = 389 mm, left) and at the edge (R = 220 mm, right) with normal (blue) and reversed (red) electric field. Pressure (a, d), temperature (b, e) and (c, f) density are shown.

versed Ohmic fields (Fig. 9). In the TST-2 configuration, we measured pressures $p_{e,\perp}$ and $p_{e,\parallel}$ ($p_{e,co}$ or $p_{e,ctr}$) by the first- and second-passes at the plasma center, respectively. We measured $p_{e,co}$ and $p_{e,ctr}$ with the second-pass in the normal and the reversed electric fields experiment, respectively. We note here that $\boldsymbol{k}_{first}$ ($\boldsymbol{k}_{second}$) is not purely perpendicular (parallel) to the magnetic field at the plasma edge (see Table 1). In Fig. 9, each symbol corresponds to one measurement of a plasma discharge. Figure 9 shows the data scatter. The ranges for plasma density, temperature and the Ohmic electric field are wide because we took measurements for several different discharge timings. These differences may be the cause of the scatter.

Figure 9 shows a clear relation of $p_{e,co} > p_{e,\perp} > p_{e,ctr}$, which is qualitatively consistent with the CQL3D code calculation. The pressure anisotropies $p_{e,\parallel}/p_{e,\perp}$ are around 30% and 100% at the plasma center and edge, respectively. Note that the anisotropy at the edge might be larger because the directions of the measurement are not purely perpendicular (parallel) to the magnetic field. The large measured anisotropy cannot be explained by the 5% and 10% measurement errors at the plasma center and edge, respectively.

Table 2 Averaged χ^2 values of the fitting. 3T and Shift indicate the three temperature-Maxwellian model and the shifted-Maxwellian model, respectively.

R [mm]	Models	n	m	$\langle\chi^2\rangle/(n-m)$	Data number
389	3T	6	2	1.55	382
389	Shift	6	2	2.01	382
220	3T	6	2	1.84	571
220	Shift	6	2	2.83	571

Furthermore, we compared the chi-squared value χ^2 of the three-temperature Maxwellian model and the shifted-Maxwellian model. χ^2 represents the goodness of fit, defined as follows:

$$\chi^2 = \sum_i \frac{(y_i - y_{\mathrm{fit},i})^2}{\sigma_i^2},$$

where y_i, $y_{\mathrm{fit},i}$, and σ_i are the Thomson scattering signal, the resultant value of fitting, and the measurement error, respectively. i is the index of a polychromator wavelength channel. We estimated σ_i from the relation in Eq. (1). The results are listed in Table 2. n and m indicate the number of wavelength channels and the number of fitting parameters, respectively. $\langle\chi^2\rangle$ denotes the averaged value of χ^2 for all data. As a result, fitting to the three-temperature Maxwellian model is better than the fitting to the shifted-Maxwellian model in both cases. However, there is a finite difference between $\langle\chi^2\rangle$ and $n - m$, which suggests that either more parameters or a more appropriate model is required.

Using the three-temperature Maxwellian model, we calculated the current density of the thermal electrons from the results shown in Fig. 9. We derived the current density j_e from Eq. (2) as

$$\begin{aligned} j_e &\equiv e \int v_\parallel f_e(v_\parallel) dv_\parallel \\ &= e\sqrt{\frac{k}{2\pi m}}\left(n_{e,co}\sqrt{T_{e,co}} - n_{e,ctr}\sqrt{T_{e,ctr}}\right). \end{aligned} \quad (3)$$

In order to investigate the dependence of j_e on the plasma resistivity η, we define η as

$$\eta = \frac{\sqrt{2}}{12\pi^{3/2}} \frac{Z_{\mathrm{eff}} e^2 m_e^{1/2}}{\epsilon_0^2 T_{e,\mathrm{first}}^{3/2}} \ln\Lambda. \quad (4)$$

Z_{eff}, e, m_e, ϵ_0 and $\ln\Lambda$ are the effective charge, the elementary charge, the electron mass, the vacuum permittivity, and the Coulomb logarithm, respectively. Here, we assume $Z_{\mathrm{eff}} = 1$.

Since only $p_{e,co}$ or $p_{e,ctr}$ can be measured for one plasma discharge, we assumed that the plasma parameters depend on $T_{e,\mathrm{first}} (\simeq T_{e,\perp})$. Then we divided the $T_{e,\mathrm{first}}$ data into every 10 eV and 5 eV intervals for the plasma center

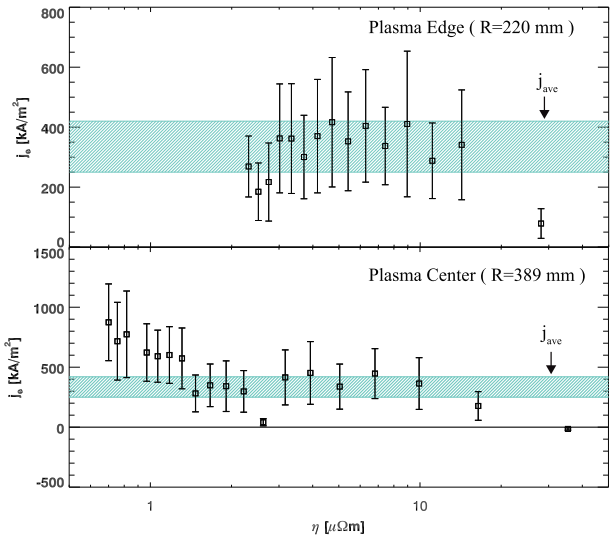

Fig. 10 The relation between j_e and η at the plasma center and the edge. Only the data of which the number of measurement is more than 10 is plotted. Sky blue hatched areas represent the range of j_{ave} in the experiments.

and edge, respectively. In each group, we averaged the corresponding $T_{e,second}$, $n_{e,first}$, and $n_{e,second}$, and then substituted the averaged values into Eqs. (3) and (4). Figure 10 shows the relations between j_e and η. The hatched areas represent the spatially-averaged current density $j_{ave} = I_p/\pi a^2$ in the experiments. The measured current density value is close to that of j_{ave}. This result suggests that the contribution of thermal electrons (not fast electrons) to the current density is relatively large in Ohmic-heated plasmas.

6. Summary

We developed a double-pass Thomson scattering diagnostic system on the TST-2, evaluated the systematic and random errors, and found the measurement error to be around 5 - 10% for plasmas with a density of 2×10^{19} m^{-3}. We observed a finite difference between pressures perpendicular and parallel to the magnetic field. The co-directed (i.e., the direction of electron acceleration) parallel pressure was almost always higher than the perpendicular pressure, and the counter-directed parallel pressure was almost always lower than the others. There was a pressure anisotropy of around 30% at the plasma center, while at the plasma edge it was around 100%. This represents the first measurement of a relatively large electron pressure anisotropy in high temperature plasmas. The fitting to the three-temperature Maxwellian model was better than to the shifted-Maxwellian model, which is qualitatively consistent with the Fokker-Planck code calculation. We calculated the electron current density of the plasma using the three-temperature model. The resulting values are close to the spatially-averaged current density, which suggests that the contribution of thermal electrons to the plasma current is relatively large in Ohmic-heated plasmas. These results contribute to the understanding of the anisotropy of electron velocity distribution functions and demonstrate the possibility of measuring current density with Thomson scattering diagnostics.

Acknowledgments

This work was supported by the Japan Society for the Promotion of Science (JSPS) Grant-in-Aid for Scientific Research Nos. 24656556 and 21226021 and by the National Institute for Fusion Science (NIFS) Collaborative Research Program No. NIFS12KUTR078.

[1] C.M. Bishop and R.J. Hastie, Nucl. Fusion **25**, No.10, 1443 (1985).
[2] J.B. Taylor, Phys. Fluids **6**, No.11, 1529 (1963).
[3] T. Matoba *et al.*, Jpn. J. Appl. Phys. **18**, 1127 (1979).
[4] R.G. Watt and Z.A. Pietrzyk, Phys. Fluids **22**, 778 (1979).
[5] E. Yatsuka *et al.*, Nucl. Fusion **51**, 123004 (2011).
[6] H. Tojo *et al.*, Rev. Sci. Instrum. **83**, 10E346 (2012).
[7] M.D. Bowden *et al.*, J. Appl. Phys. **73**, No.6, 2732 (1993).
[8] I.H. Hutchinson, J. Phys. D: Appl. Phys. **10**, L11 (1977).
[9] A.C.A.P. Van Lammeren *et al.*, Nucl. Fusion **32**, No.4, 655 (1992).
[10] Y. Yagi *et al.*, Plasma Phys. Control. Fusion **33**, No.12, 1391 (1991).
[11] L. Pieroni and S.E. Segre, Phys. Rev. Lett. **34**, No.15, 928 (1975).
[12] F.A. Karelse *et al.*, Plasma Phys. Control. Fusion **43**, 443 (2001).
[13] J. Hiratsuka *et al.*, Plasma Fusion Res. **6**, 1202133 (2011).
[14] J. Hiratsuka *et al.*, Plasma Fusion Res. **7**, 2402092 (2012).
[15] Y. Takase *et al.*, Nucl. Fusion **41**, 1543 (2001).
[16] A. Ejiri *et al.*, Plasma Fusion Res. **5**, S2082 (2010).
[17] N. Singh, Plasma Phys. **20**, 927 (1978).
[18] R.W. Harvey and M.G. McCoy, "CQL3D Fokker-Planck code", in Proceedings of the IAEA Technical Committee Meeting on Simulation and Modeling of Thermonuclear Plasmas, Montreal, Canada, 1992 (USDOC NTIS Document No. DE93002962).